CHAPTER 4

X–RAY DIFFRACTION AND SCANNING ELECTRON MICROSCOPY ANALYSIS

4.1 Introduction

After the films have been prepared it is important to know whether the films are amorphous or crystalline or both and to characterize morphology of the films. This information may shed some light on the conductivity of the samples. This can be done using x–ray diffraction (XRD) and scanning electron microscopy (SEM) respectively.

Kumutha *et al*, (2005, 2006), Ali *et al*, (2006, 2008) and Hashim *et al*, (2010) have reported that homogeneous polymer with good mechanical strength can be prepared using MG30 polymer. Kumutha *et al.* (2005) have used MG30 with ethylene carbonate (EC) as plasticizer and Al_2SiO_5 as filler. Ali *et al*. (2006, 2008) have introduced propylene carbonate (PC) and ethylene carbonate (EC) to MG30 added with lithium salt to enhance the conductivity. Hashim *et al*. (2010) have explored the potential application of MG30 incorporated with LiTf and silicon dioxide (SiO_2) as an electrolyte for lithium polymer battery.

4.2 X–ray diffractogram of MG30–$LiCF_3SO_3$ films

Using the compositions mentioned in Chapter Three, all the MG30 based polymer electrolytes were x–rayed and the results are depicted. Low *et al.* (2010, 2011)

and Su'ait *et al.* (2009) have reported that homogenous polymer can be achieved in natural rubber grafted PMMA polymer, MG49. However, there is no XRD report on the MG30 based polymer electrolytes.

Figure 4.1 shows the x–ray diffraction patterns of pure LiTf, MG30 and MG30 added with different amounts of $LiCF_3SO_3$. Sharp diffraction peaks at $2\theta = 9.6°$, 16.3°, 19.8°, 20.6°, 22.9°, 24.7°, 32.9°, 33.6°, 40.1° and 41.8° reveal the crystalline nature of pure $LiCF_3SO_3$ (Figure 4.1 (k)). It can be inferred that the all MG30 based samples are quite amorphous as broad peaks could be observed between $2\theta = 10°$ to 25° and centered at $2\theta = 17.3°$. Some crystalline peaks though not of high intensity could be observed in the XRD patterns which could imply the ability of the MG30 polymer to retain the salt within its structure (Saikia and Kumar, 2004; Rajendran et al., 2008). However, the diffractogram of the samples with 40 and 45 wt. % $LiCF_3SO_3$ showed a small peak at $2\theta = 22.7°$ and a relatively broad peak at $2\theta = 21°$ to 23° and these indicate the presence of excessive $LiCF_3SO_3$ salt precipitation.

The highly amorphous nature of the samples implies that the carbonyl (C=O) and carboxyl (–COO) groups of PMMA have interacted with Li^+ ions from the salt. Kumutha *et al.* (2006) stated that the oxygen atom in the carbonyl functional group of PMMA can form coordinate bonding with the lithium ions from the added salt. The peak observed at $2\theta = 21°$ to 23° can be attributed to $LiCF_3SO_3$ since there is a peak due to $LiCF_3SO_3$ at $2\theta = 22.9°$ in its diffractogram. The peak at lower 2θ angle at 9.8° is also probably due to the pure $LiCF_3SO_3$ peak at 9.6°. These peaks are slightly shifted in the diffractogram of the polymer–salt complex.

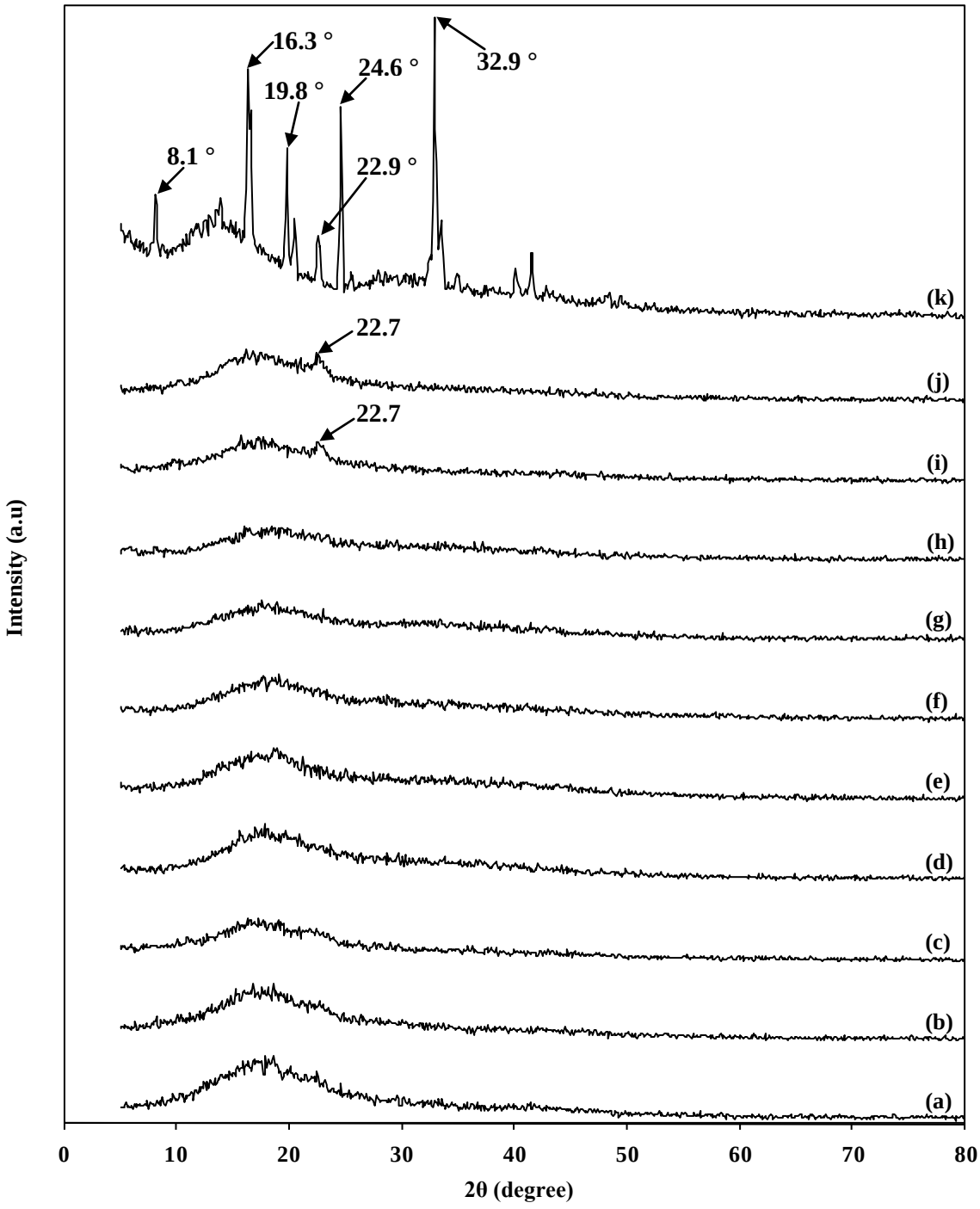

Figure 4.1 XRD diffractograms of (a) MG0L, (b) MG5L, (c) MG10L, (d) MG15L, (e) MG20L, (f) MG25L, (g) MG30L, (h) MG35L, (i) MG40L, (j) MG45L and (k) $LiCF_3SO_3$

Figure 4.2 shows some of the deconvoluted XRD results for the $LiCF_3SO_3$–MG30 systems.

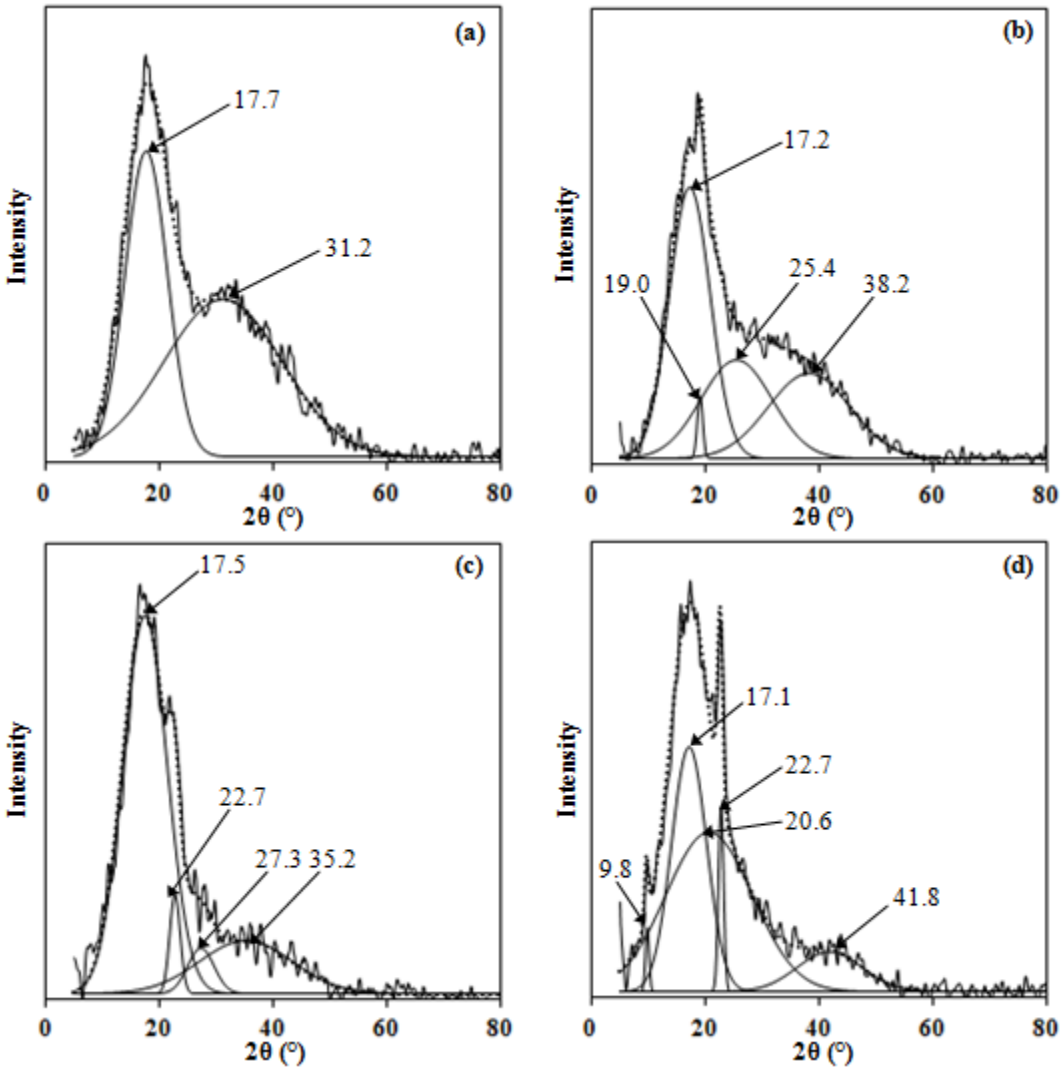

Figure 4.2 Deconvoluted XRD results of (a) MG0L, (b) MG10L, (c) MG30L and (d) MG40L

According to Hodge *et al.* (1996), the crystalline fractions in samples can be predicted from the ratio of the integrated area of peaks associated with crystalline reflections to the integrated area of the spectrum by the equation below:

$$X_C = {A_C}/{A_T} \times 100\% \qquad (4.1)$$

Table 4.1: Degree of crystallinity data of the MG30–$LiCF_3SO_3$ samples

Sample	A_T	A_C	X_C (%)
MG10L	0.43	0.0064	1.50
MG15L	0.46	0.0069	1.49
MG20L	0.56	0.0133	2.39
MG25L	0.39	0.0096	2.46
MG30L	0.38	0.0110	2.92
MG35L	0.39	0.0155	3.93
MG40L	0.45	0.0186	4.16
MG45L	0.37	0.0174	4.68

Here X_C is the crystalline fraction, A_T and A_C are the total and crystalline peak areas respectively.

As shown in Figure 4.2 (a), two broad peaks are observed centred at 2θ = 17.7° and 31.2° for MG0L (pure MG30). These peaks broadened with reduced intensity and are shifted from 2θ = 17.7° to the values at between 17.1° to 17.5° for MG10L, MG30L and MG40L. This shift indicates occurrence of complexation between the polymer and lithium salt (Sivakumar *et al.*, 2006 and Austin Suthanthiraj, 2011a). Some sharp and small peaks have been observed when the $LiCF_3SO_3$ was incorporated in the MG30 films. In Figure 4.2(d), a few more characteristic peaks of $LiCF_3SO_3$ are observed in MG40L at 2θ = 22.7° and 9.8°. From the deconvoluted XRD pattern it can be concluded that the salt has therefore recrystallized out of the MG40L film. However, it can be concluded that all the samples are amorphous because the percentage of crystalinity for all samples is below 5%.

4.3 X–ray diffractogram of MG30–$LiCF_3SO_3$–$LiN(CF_3SO_2)_2$ films

Figure 4.3 shows the x–ray diffractograms for all $LiCF_3SO_3$–$LiN(CF_3SO_2)_2$ doped MG30 films.

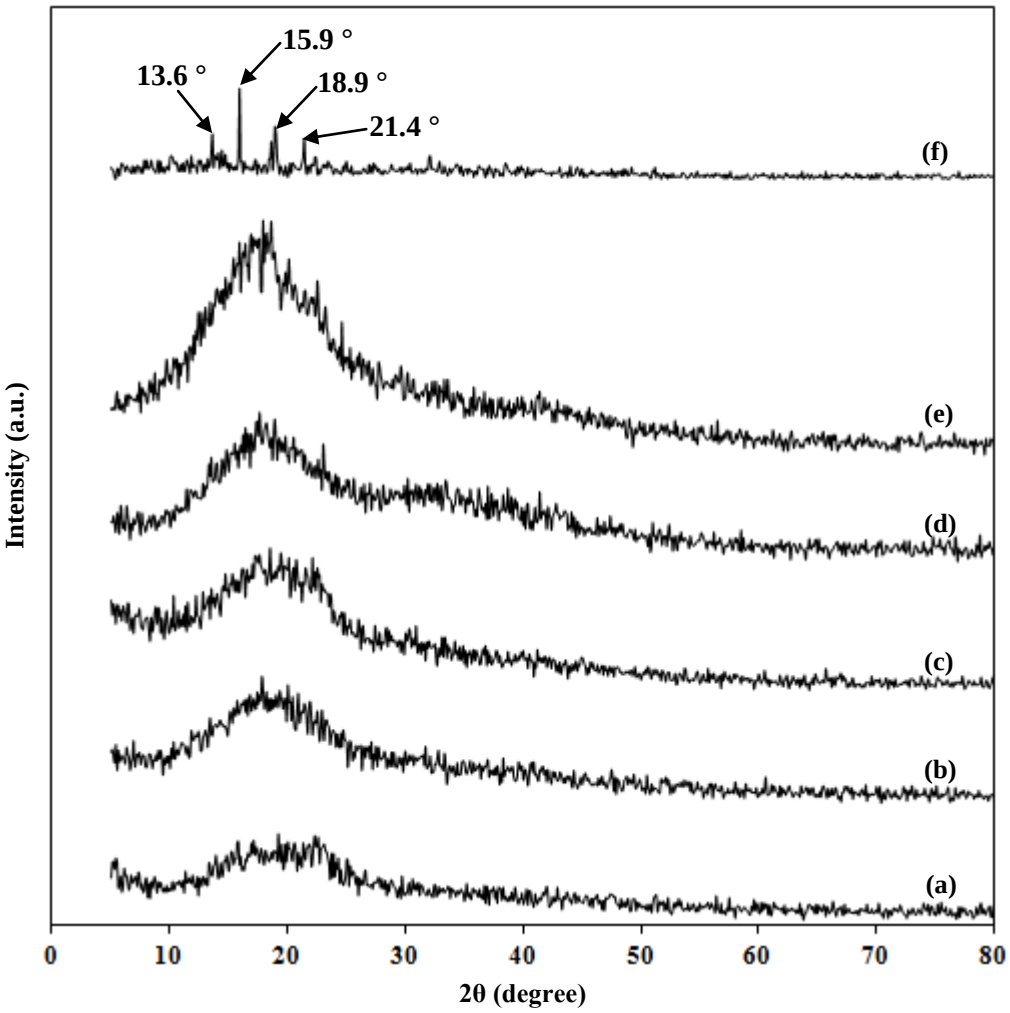

Figure 4.3 X–ray diffractograms of (a) MG15L15I, (b) MG20L10I, (c) MG10L20I, (d) MG30L, (e) MG0L and (f) $LiN(CF_3SO_2)_2$

Figure 4.3 (f) reveals the crystalline peaks of $LiN(CF_3SO_2)_2$ at 2θ = 13.6°, 15.9°, 18.9° and 21.4°. All the samples are quite amorphous because broad peaks could be observed between 2θ = 10° to 30°. Some small crystalline peaks can be observed in the XRD patterns which could imply the ability of the MG30 polymer to retain most of the salt within its structure. The oxygen atom in the carbonyl (C=O) and carboxyl (–COO) functional groups of PMMA can form coordinate bonding with the lithium ions from the incorporating salt. The interaction between Li^+ ions and oxygen atoms has been confirmed by FTIR studies in this work. Figure 4.4 shows some of the deconvoluted XRD results for the $LiCF_3SO_3$–$LiN(CF_3SO_2)_2$–MG30 systems.

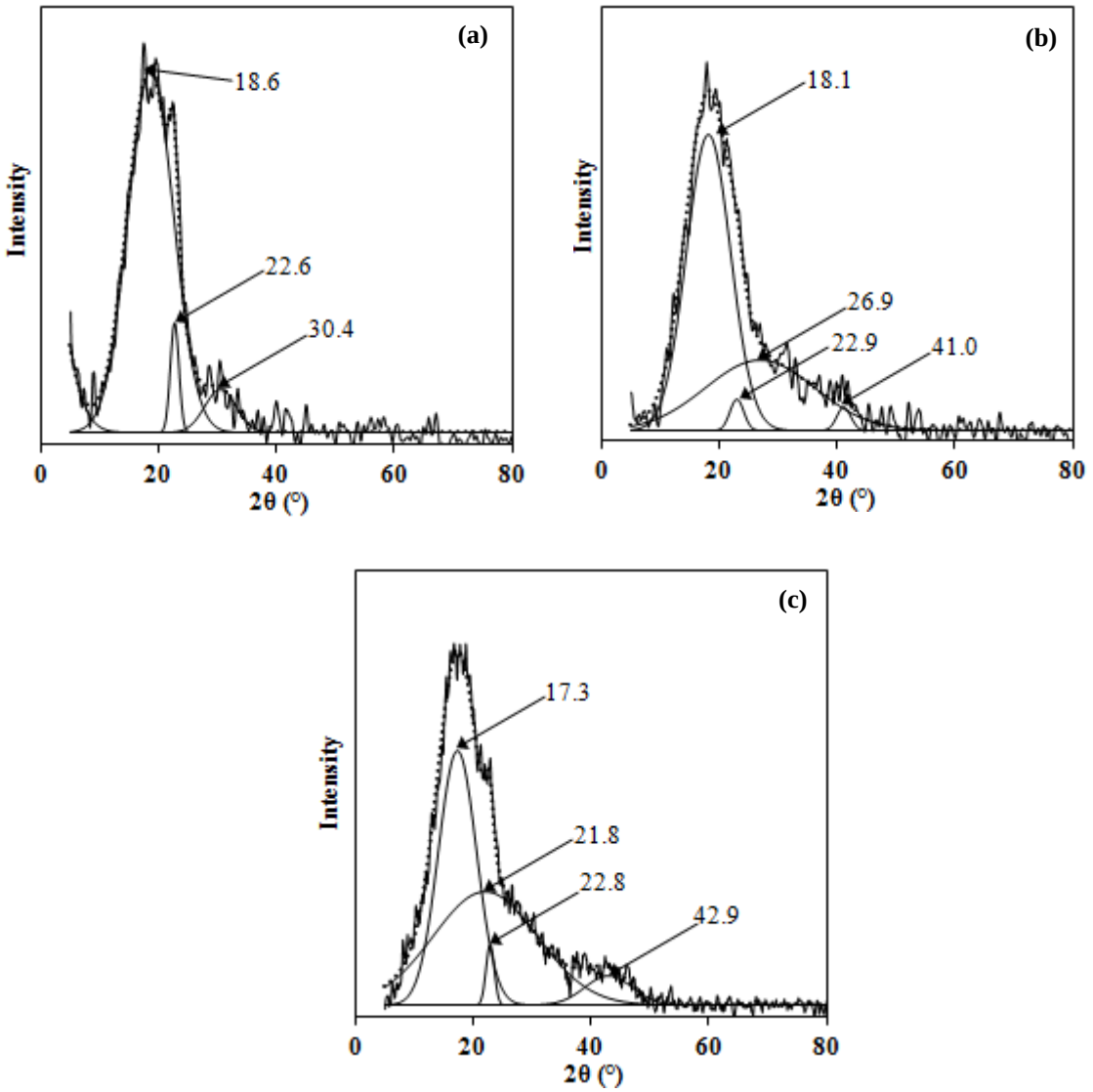

Figure 4.4 Deconvoluted XRD results of (a) MG20L10I (b) MG15L15I and (c) MG10L20I

As shown in Figure 4.4, the double salt MG30 samples contain mainly broad deconvoluted peaks that can be observed in the diffractogram of the polymer blends. Therefore, it can be concluded that the double lithium salt were successfully incorporated in the MG30 polymer. These peaks become broader with reduced intensity and are shifted to 2θ values centred at 18.1° and 26.9° for MG15L15I in Figure 4.2 (b) as compared to Figure 4.2 (a) and (c). This bigger difference in shift between peaks of MG15L15I and original MG30 peaks indicates the interaction between polymer and lithium salts. However, a characteristics peak of the $LiCF_3SO_3$ can be observed at around 22.8°. The intensity of the peak is lowest in the diffractogram of MG15L15I,

followed by the intensity of the same peak in the diffractogram of MG10L20I and finally that of MG20L10I.

The degree of crystallinity of the MG30–$LiCF_3SO_3$–$LiN(CF_3SO_2)_2$ samples were evaluated using the equation 4.1 and listed in Table 4.2. The calculated region is area under the peak located around 22.7°.

Table 4.2: Degree of crystallinity data of the MG30–$LiCF_3SO_3$–$LiN(CF_3SO_2)_2$ samples

Sample	A_T	A_C	X_C (%)
MG15L15I	0.29	0.0069	2.37
MG20L10I	0.25	0.0064	2.57
MG10L20I	0.31	0.0088	2.83

4.4 X–ray diffractogram of MG30–$LiCF_3SO_3$–PEG200 films

Figure 4.5 depicts the x–ray diffractograms for MG30–$LiCF_3SO_3$–PEG200 films. It can be inferred that all samples are highly amorphous as broad peaks could be observed between $2\theta = 5°$ to 25°, which is due to the ability of the MG30 polymer to retain the salt within its almost fully amorphous nature structure. A new, but peak located at 22.4° is observed in the diffractogram of PEG200 added samples.

The deconvoluted XRD results are illustrated in Figure 4.6. As mentioned before, the samples are mainly amorphous in nature and the percentage of crystalline phases for samples with PEG200 concentration from 5 to 30 wt. % is found to be less than 5 %.

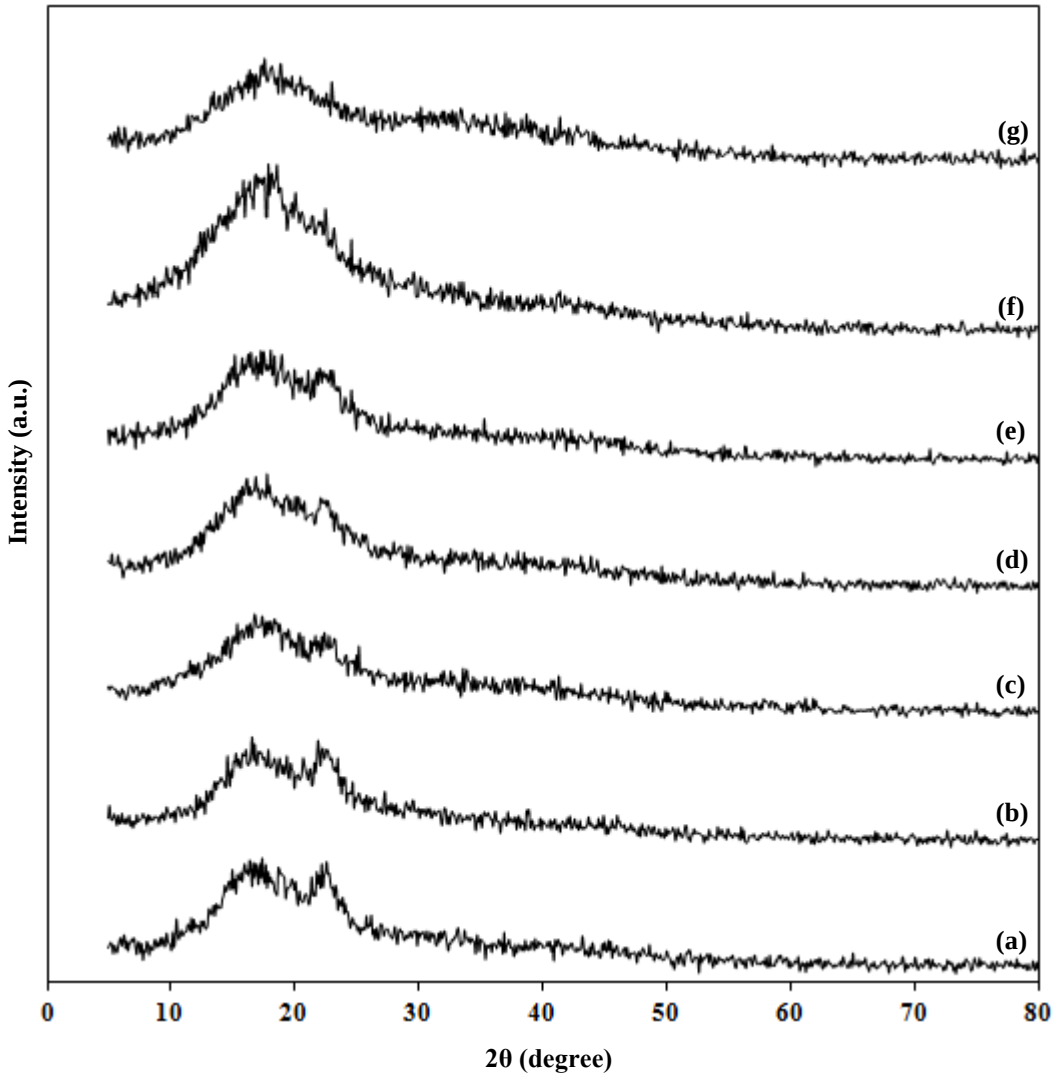

Figure 4.5 X–ray diffractograms of (a) MG30L–5P, (b) MG30L–7P, (c) MG30L–10P, (d) MG30L–20P, (e) MG30L–30P, (f) pure MG30 (g) MG30L

The degree of crystallinity of the MG30–$LiCF_3SO_3$–PEG200 samples was evaluated using the equation 4.1 and the results are listed in Table 4.3. The calculated crystalline region is the area under the peak located around 22.7 °.

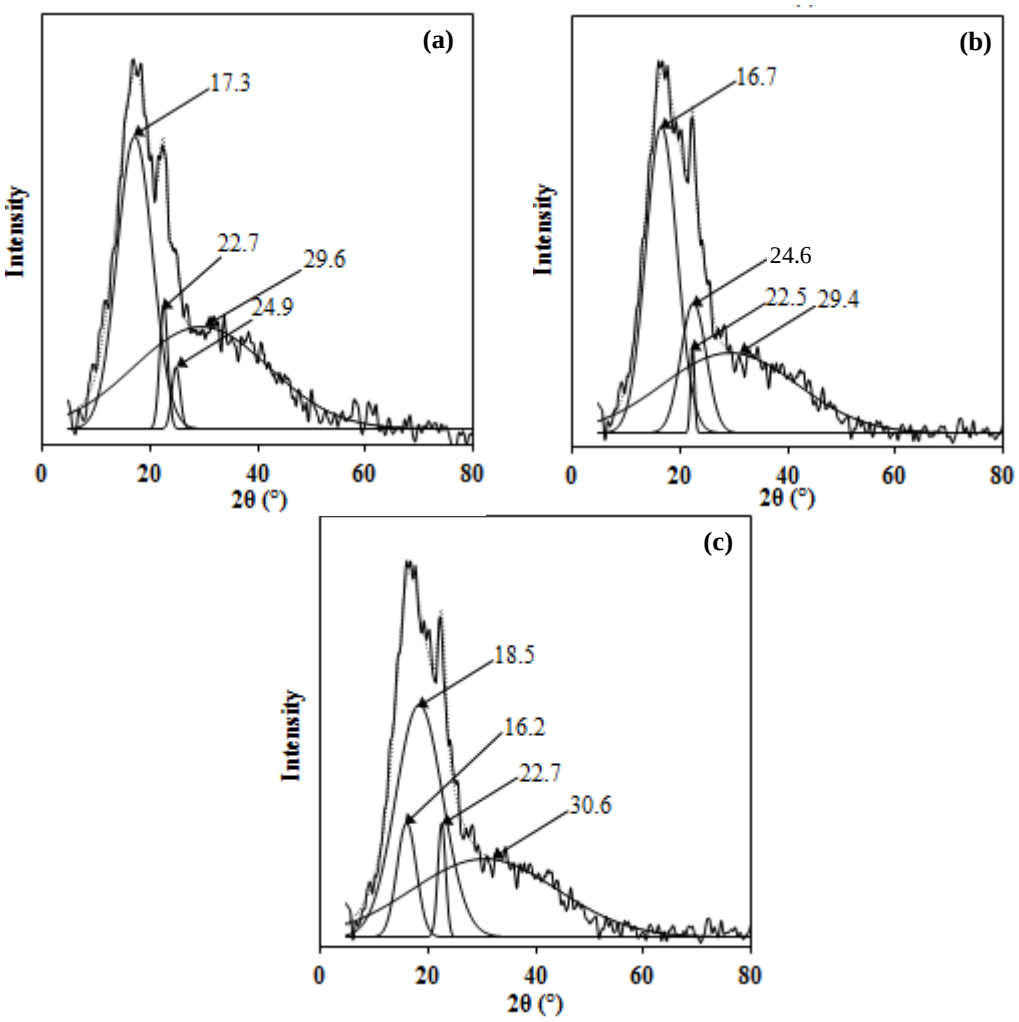

Figure 4.6 Deconvoluted XRD results of (a) MG30L–7P, (b) MG30L–10P and (c) MG30L–20P

Table 4.3: Degree of crystallinity data of MG30–$LiCF_3SO_3$–PEG200 samples

Sample	A_C	A_T	X_C (%)
MG30–5P	0.0341	0.8815	3.87
MG30–7P	0.0282	0.8013	3.52
MG30–10P	0.0158	0.8951	1.77
MG30–20P	0.0230	0.9245	2.49
MG30–30P	0.0245	0.9018	2.72

4.5 Scanning Electron Microscope (SEM)

To the author's knowledge, there are only two reports on the SEM analysis on the PMMA grafted natural rubber, MG49 which carried out by Low *et al.* (2010) and (2011). This prompts the author to carry out the research on SEM for the MG30 with the hope to add some knowledge to the growing literature on PMMA grafted NR.

4.5.1 SEM of MG30–$LiCF_3SO_3$ films

Figures 4.7 (a) to (g) depict SEM micrographs of $LiCF_3SO_3$ doped MG30 at 1000 X magnification. MG30 films doped up to 25 wt. % $LiCF_3SO_3$ were observed to have smooth surface with some burnt marks. The sample which contained 30 wt. % $LiCF_3SO_3$ has a smooth surface. The smooth morphology is related to the reduction of crystallinity of the highly amorphous polymer host with the presence of $LiCF_3SO_3$. Again this micrograph may serve as additional evidence that the salt has completely dissolved in the matrix. The micrographs of samples containing 35 and 40 wt. % $LiCF_3SO_3$ show the surfaces to be porous and containing solid structures. These solid structures can be recrystallized $LiCF_3SO_3$ since some small peaks due to $LiCF_3SO_3$ can be observed in the diffractogram of the sample. More peaks of $LiCF_3SO_3$ can be observed in the diffractogram of the sample with 40 wt. % salt. The micrograph of this sample (containing 40 wt. % $LiCF_3SO_3$) shows a more porous morphology with solid structures filled in them. The formation of the pores may be due to the increase in viscosity as a result of increment in salt concentration which delayed the liquid solution from joining together to form a continuing surface. To the authors' knowledge, no reports have shown the appearance of such structures at the surface of the film for natural rubber based electrolytes.

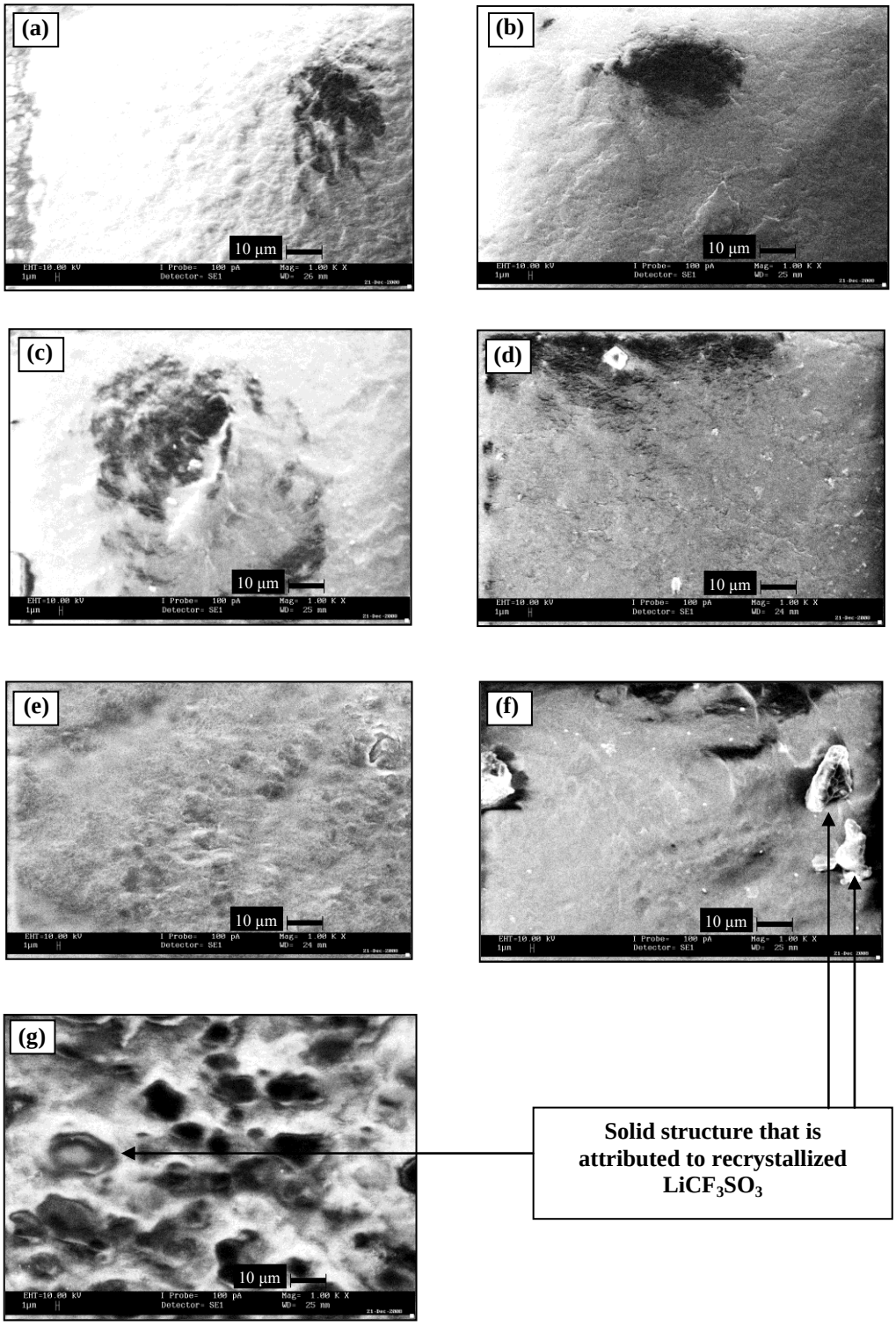

Figure 4.7 SEM micrographs at 1000X magnification of (a) MG10L, (b) MG15L, (c) MG20L, (d) MG25L, (e) MG30L, (f) MG35L and (g) MG40L

4.5.2 SEM of MG30–$LiCF_3SO_3$–$LiN(CF_3SO_2)_2$ films

Figures 4.8 (a) to (c) depicts SEM micrographs of films comprising MG30, $LiCF_3SO_3$ and $LiN(CF_3SO_2)_2$ at 1000 X magnification. For the samples MG20L10I and MG10L20I the surface appears rough with bulging structures on the surface. These structures may be attributed to ion aggregates. The micrographs of the sample containing 70 wt. % MG30 incorporated with 15 wt. % $LiN(CF_3SO_2)_2$ and 15 wt. % $LiCF_3SO_3$ shows a smoother morphology.

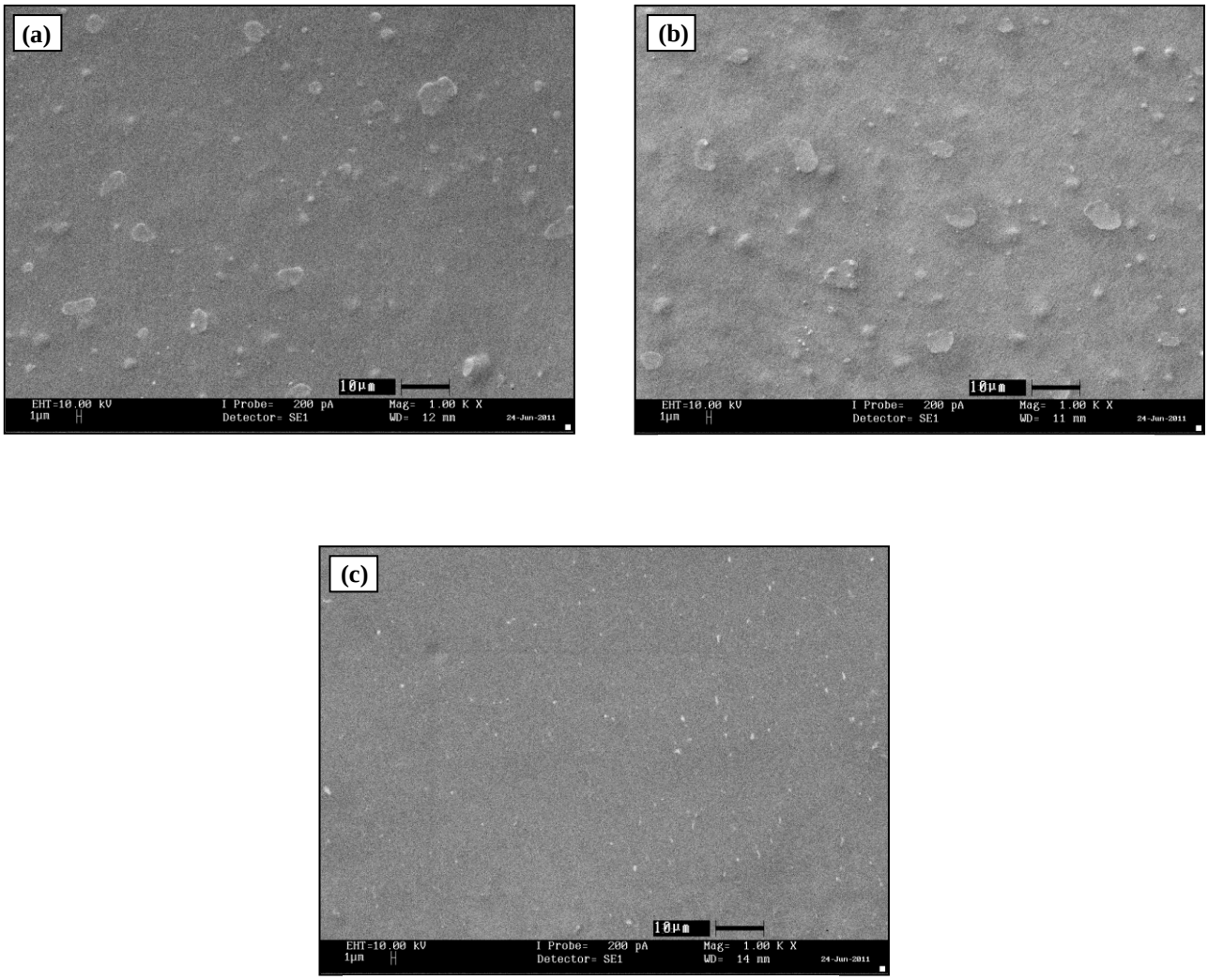

Figure 4.8 SEM micrographs at 1000X magnification of (a) MG10L20I, (b) MG20L10I and (c) MG15L15I

4.5.3 SEM of MG30–$LiCF_3SO_3$–PEG200 films

Figure 4.9 shows the SEM pictures for the MG30–$LiCF_3SO_3$–PEG200 films. It is clear that the films appear to have a smooth surface when the content of PEG200 is less than 10 wt. %. Some small spherical particles can be observed for the MG30–20P and getting more obvious in the MG30–30P sample. This may be due to overloading of PEG200 to blend with MG30. A comparable smooth and clear surface has been observed in Figure 4.6 (c) which is believed to be the best candidate among others in terms of conductivity.

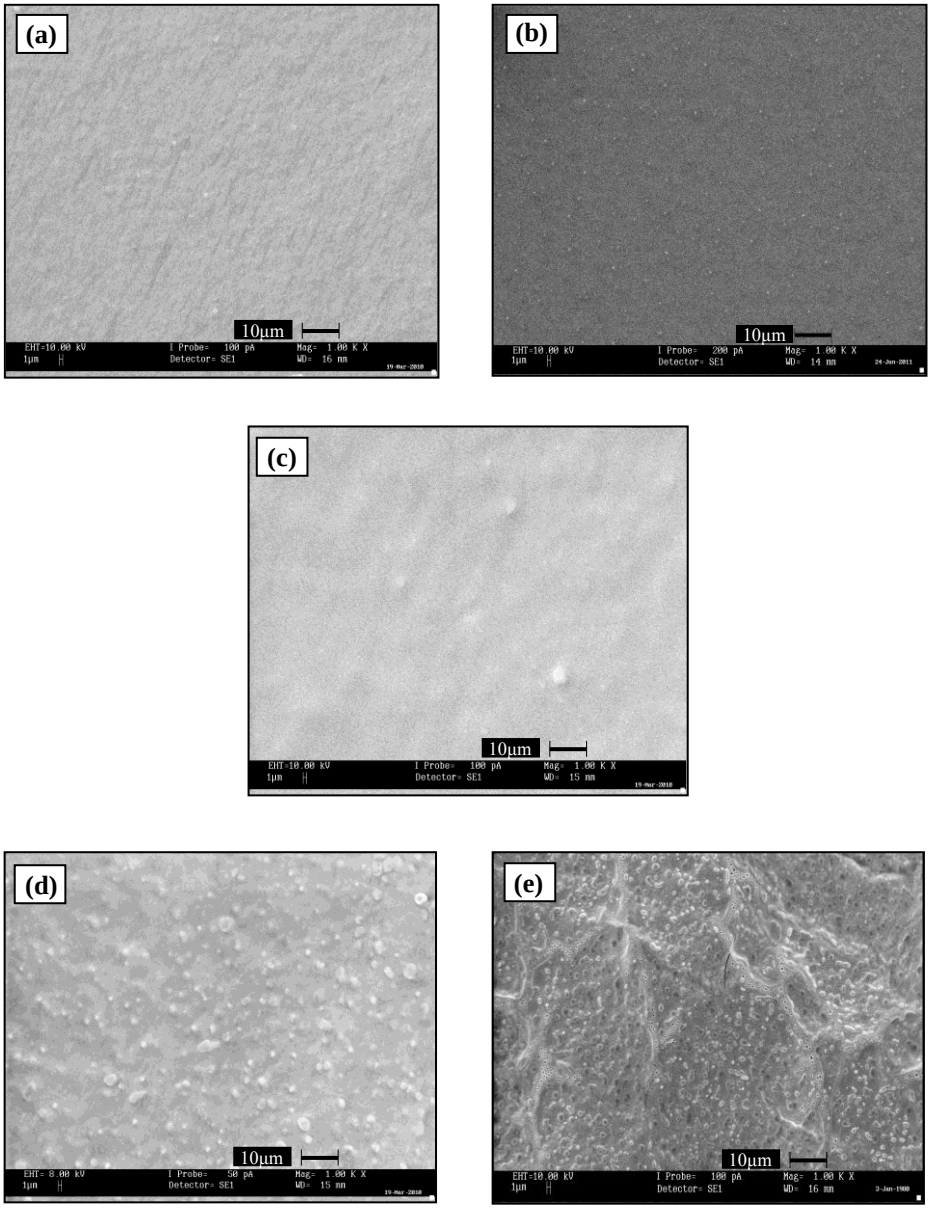

Figure 4.9 SEM micrographs at 1000X magnification of (a) MG30L–5P, (b) MG30L–7P, (c) MG30L–10P, (d) MG30L–20P and (e) MG30L–30P

4.6 Summary

From X–ray diffraction and SEM analysis of all the MG30 based polymer electrolytes, it can be predicted that the MG15L15I and MG30–10P membrane being the most amorphous and homogenous films among all other samples within their systems to exhibit the highest room temperature electrical conductivity. The MG30 film has the smoothest morphology but it is not the most amorphous film. However, since it has more salt content compared to MG10L, MG15L, MG20L and MG25L, it is still predicted to exhibit the highest room temperature electrical conductivity.